Ultrafast carrier relaxation and vertical-transport phenomena in semiconductor superlattices: A Monte Carlo analysis

Ultrafast carrier relaxation and vertical-transport phenomena in semiconductor superlattices: A Monte Carlo analysis

F. Rossi, T. Meier, P. Thomas, and S.W. Koch
Fachbereich Physik und Zentrum für Materialwissenschaften, Philipps-Universität Marburg, Renthof 5, D-35032 Marburg, Germany

P.E. Selbmann and E. Molinari
Istituto Nazionale di Fisica della Materia INFM e Dipartimento di Fisica, Università di Modena, Via Campi 213/A, I-41100 Modena, Italy
(Received 25 January 1995; revised manuscript received 14 February 1995)

The ultrafast dynamics of photoexcited carriers in semiconductor superlattices is studied theoretically on the basis of a Monte Carlo solution of the coupled Boltzmann transport equations for electrons and holes. The approach allows a kinetic description of the relevant interaction mechanisms such as intraminiband and interminiband carrier-phonon scattering processes. The energy relaxation of photoexcited carriers, as well as their vertical transport, is investigated in detail. The effects of the multiminiband nature of the superlattice spectrum on the energy relaxation process are discussed with particular emphasis on the presence of Bloch oscillations induced by an external electric field. The analysis is performed for different superlattice structures and excitation conditions. It shows the dominant role of carrier–polar-optical-phonon interaction in determining the nature of the carrier dynamics in the low-density limit. In particular, the miniband width, compared to the phonon energy, turns out to be a relevant quantity in predicting the existence of Bloch oscillations.

I. INTRODUCTION

The technological progress in the generation of ultrashort laser pulses, together with the possibility to detect processes on this time scale, has led to a series of experiments that gave insight into the microscopic carrier dynamics in a semiconductor. A phenomenon that has been widely investigated during the past few years is the energy relaxation of photoexcited carriers,[1–4] which typically occurs on a picosecond or femtosecond time scale. Different experimental techniques have been used: luminescence experiments, either band to band,[1,2] where the product of the distribution functions in the valence and the conduction bands both contribute, or band-to-acceptor,[3] which is most sensitive to the electron distribution, as well as pump-and-probe experiments,[4] which yield information on the sum of the distribution functions. On the other hand, recent progress in the fabrication and characterization of semiconductor heterostructures and superlattices allows a detailed investigation of another class of phenomena such as Bloch oscillations[5] (BO's) and the corresponding terahertz radiation,[6] which may arise due to the application of an external electric field.

Besides attempts of direct integration of the quantum kinetic equations,[7–10] the most commonly used approach for the theoretical analysis of energy-relaxation experiments in bulk semiconductors[1] and in low-dimensional structures[11] is the Monte Carlo method.[12] This has proven to be a powerful technique for the analysis of energy-relaxation and transport phenomena,[13] as it allows one to include on a kinetic level a large variety of scattering processes (carrier-phonon, carrier-carrier, carrier-plasmon, inter-valence-band, intervalley, etc.). The role of these scattering processes in turn is influenced by the choice of the experimental conditions: carrier-carrier scattering and hot-phonon effects strongly depend on the density and intervalley transitions are suppressed if the excitation is below the threshold for this process. Thus the combination of experimental results and "simulated experiments" provides detailed information on the relevant scattering rates and coupling constants.

In this paper we give a theoretical analysis of the ultrafast intraband dynamics of photoexcited carriers in semiconductor superlattices. Our approach is based on a Monte Carlo solution of the coupled set of Boltzmann transport equations describing the ultrafast electron and hole dynamics within a multiminiband scheme.[14]

We present a detailed investigation of the energy relaxation of photoexcited carriers and of their vertical transport within a superlattice structure. The energy-relaxation analysis will show the existence of different relaxation times corresponding to the different interminiband and intraminiband scattering mechanisms. On the other hand, the vertical transport analysis will clearly show the dominant role of carrier–polar-optical-phonon interaction in determining the carrier dynamics: for superlattice structures characterized by a miniband width less than the optical-phonon energy and for laser excitations close to the band gap, the carrier dynamics exhibits Bloch oscillations; on the contrary, for miniband widths greater than the phonon energy or for laser excitations

far from the band gap, the carrier-phonon scattering results in a strong damping of such charge oscillations.[15]

The paper is organized as follows. In Sec. II the physical system and the theoretical approach are introduced. In Sec. III we describe the Monte Carlo procedure for the solution of the set of Boltzmann transport equations. In Sec. IV the results of our Monte Carlo simulations are presented and discussed. Finally, in Sec. V we will draw some conclusions.

II. PHYSICAL SYSTEM AND THEORETICAL APPROACH

In order to study the ultrafast dynamics of photoexcited carriers in semiconductor superlattices, let us consider a physical system described by the following Hamiltonian:

$$\mathbf{H} = (\mathbf{H}_c + \mathbf{H}_\mathbf{F} + \mathbf{H}_p) + (\mathbf{H}_{cp} + \mathbf{H}_{cl}) = \mathbf{H}_0 + \mathbf{H}' \ . \quad (1)$$

Here

$$\mathbf{H}_c = \mathbf{H}_c^e + \mathbf{H}_c^h = \sum_{\mathbf{k}\nu} \mathcal{E}^e_{\mathbf{k}\nu} c^\dagger_{\mathbf{k}\nu} c_{\mathbf{k}\nu} + \sum_{\mathbf{k}\nu} \mathcal{E}^h_{-\mathbf{k}\nu} d^\dagger_{-\mathbf{k}\nu} d_{-\mathbf{k}\nu} \quad (2)$$

is the free-carrier Hamiltonian written in the usual electron-hole picture where $\mathbf{k}$ and ν denote, respectively, the carrier wave vector and the miniband index while $\mathcal{E}^{e(h)}_{\mathbf{k}\nu}$ denotes the electron (hole) band structure of the superlattice. The $c^\dagger_{\mathbf{k}\nu}$ ($c_{\mathbf{k}\nu}$) and $d^\dagger_{-\mathbf{k}\nu}$ ($d_{-\mathbf{k}\nu}$) are the creation (annihilation) operators of electrons and holes with wave vector $\mathbf{k}$ in miniband ν. The term

$$\mathbf{H}_\mathbf{F} = \mathbf{H}^e_\mathbf{F} + \mathbf{H}^h_\mathbf{F} = \sum_{\mathbf{k}\nu,\mathbf{k}'\nu'} \alpha^e_{\mathbf{k}\nu,\mathbf{k}'\nu'} c^\dagger_{\mathbf{k}\nu} c_{\mathbf{k}'\nu'} + \sum_{\mathbf{k}\nu,\mathbf{k}'\nu'} \alpha^h_{\mathbf{k}\nu,\mathbf{k}'\nu'} d^\dagger_{-\mathbf{k}\nu} d_{-\mathbf{k}'\nu'} \quad (3)$$

describes the effect of a homogeneous applied electric field $\mathbf{F}$; the quantities $\alpha^{e(h)}_{\mathbf{k}\nu,\mathbf{k}'\nu'}$ denote the matrix elements of the corresponding scalar potential $-\mathbf{F}\cdot\mathbf{r}$ in our $\mathbf{k}\nu$ representation. The analysis in Refs. 16 and 17 shows that the above Hamiltonian can always be split into an intraband part ($\nu = \nu'$), which gives rise to an acceleration of the carriers within the same band, and an interband part ($\nu \neq \nu'$), which describes interband transitions induced by the external field, i.e., Zener tunneling.
The term

$$\mathbf{H}_p = \sum_\mathbf{q} \hbar\omega_\mathbf{q} b^\dagger_\mathbf{q} b_\mathbf{q} \quad (4)$$

describes the free-phonon dynamics; as usual, $b^\dagger_\mathbf{q}$ ($b_\mathbf{q}$) denotes the creation (annihilation) operator of phonons with wave vector $\mathbf{q}$ while $\omega_\mathbf{q}$ is the phonon dispersion. For simplicity, we consider a single phonon mode only; the generalization, if necessary, is obvious.

The last two contributions in (1) correspond to carrier-phonon and carrier-light interaction, respectively. The first one is given by

$$\begin{aligned}\mathbf{H}_{cp} &= \mathbf{H}^e_{cp} + \mathbf{H}^h_{cp} \\ &= \sum_{\mathbf{k}\nu,\mathbf{k}'\nu';\mathbf{q}} \left[g^e_{\mathbf{k}\nu,\mathbf{k}'\nu';\mathbf{q}} c^\dagger_{\mathbf{k}\nu} b^\dagger_\mathbf{q} c_{\mathbf{k}'\nu'} + g^{e*}_{\mathbf{k}\nu,\mathbf{k}'\nu';\mathbf{q}} c^\dagger_{\mathbf{k}'\nu'} b_\mathbf{q} c_{\mathbf{k}\nu} \right] \\ &\quad + \sum_{\mathbf{k}\nu,\mathbf{k}'\nu';\mathbf{q}} \left[g^h_{\mathbf{k}\nu,\mathbf{k}'\nu';\mathbf{q}} d^\dagger_{-\mathbf{k}\nu} b^\dagger_\mathbf{q} d_{-\mathbf{k}'\nu'} + g^{h*}_{\mathbf{k}\nu,\mathbf{k}'\nu';\mathbf{q}} d^\dagger_{-\mathbf{k}'\nu'} b_\mathbf{q} d_{-\mathbf{k}\nu} \right] . \end{aligned} \quad (5)$$

Here the quantities g denote the matrix elements of the phonon electrostatic potential in the $\mathbf{k}\nu$ representation. Their explicit form for our superlattice model will be evaluated at the end of this section. As we will see, the above Hamiltonian is responsible for both intraminiband ($\nu = \nu'$) and interminiband ($\nu \neq \nu'$) carrier-phonon scattering processes. Finally,

$$\mathbf{H}_{cl} = -\sum_{\mathbf{k},\nu\nu'} \left[\mu_{\mathbf{k},\nu\nu'} E^+(t) c^\dagger_{\mathbf{k}\nu} d^\dagger_{-\mathbf{k}\nu'} + \mu^*_{\mathbf{k},\nu\nu'} E^-(t) d_{-\mathbf{k}\nu'} c_{\mathbf{k}\nu} \right] \quad (6)$$

describes the dipole coupling of the carrier system to a laser field

$$E(t) = E^+(t) + E^-(t) = E_0(t) e^{i\omega_l t} + E_0(t) e^{-i\omega_l t} \quad (7)$$

within the usual rotating-wave approximation. The quantity $\mu_{\mathbf{k}\nu\nu'}$ is the optical matrix element between the electron and hole states while $E_0(t)$ and ω_l denote, respectively, the shape and the central frequency of the light field.

Let us now introduce the set of kinetic variables used to describe the carrier system within our semiconductor superlattice. We choose the various electron and hole distribution functions corresponding to the different conduction and valence minibands, respectively:

$$f^e_{\mathbf{k}\nu} = \langle c^\dagger_{\mathbf{k}\nu} c_{\mathbf{k}\nu} \rangle \ , \qquad f^h_{\mathbf{k}\nu} = \langle d^\dagger_{-\mathbf{k}\nu} d_{-\mathbf{k}\nu} \rangle \ . \quad (8)$$

As usual, these distribution functions are given as the $\mathbf{k}$- and ν-diagonal elements of the single-particle density matrix. In this paper, we will not pay attention to coherent interband phenomena, which are known to play a dominant role in the excitonic regime.[18] This would require us to consider also the various interband and interminiband

polarizations as kinetic variables as described in Refs. 19–22. This approach has recently been extended in order to include, in addition to the coherent phenomena, also a kinetic treatment of incoherent scattering processes by means of a generalized Monte Carlo approach.[23,24]

Let us now discuss the time evolution of the above kinetic variables in terms of their dynamic equations

$$\frac{d}{dt}f^{e}_{\mathbf{k}\nu} = \frac{1}{i\hbar}\langle[c^{\dagger}_{\mathbf{k}\nu}c_{\mathbf{k}\nu},\mathbf{H}]\rangle,$$
$$\frac{d}{dt}f^{h}_{\mathbf{k}\nu} = \frac{1}{i\hbar}\langle[d^{\dagger}_{-\mathbf{k}\nu}d_{-\mathbf{k}\nu},\mathbf{H}]\rangle\ . \tag{9}$$

According to the separation $\mathbf{H}=\mathbf{H}_0+\mathbf{H}'$ in (1), we can identify two different contributions in the equations of motion of the distribution functions:

$$\frac{d}{dt}f^{e/h}_{\mathbf{k}\nu} = \frac{d}{dt}f^{e/h}_{\mathbf{k}\nu}\Big|_{\mathbf{H}_0} + \frac{d}{dt}f^{e/h}_{\mathbf{k}\nu}\Big|_{\mathbf{H}'}. \tag{10}$$

If we neglect the interminiband terms in (3), i.e., interminiband Zener transitions, the time evolution induced by the Hamiltonian $\mathbf{H}_0$ can be evaluated exactly:[16,18]

$$\frac{d}{dt}f^{e/h}_{\mathbf{k}\nu}\Big|_{\mathbf{H}_0} = -\dot{\mathbf{k}}\cdot\nabla_{\mathbf{k}}f^{e/h}_{\mathbf{k}\nu} = -\frac{e^{e/h}\mathbf{F}}{\hbar}\cdot\nabla_{\mathbf{k}}f^{e/h}_{\mathbf{k}\nu}. \tag{11}$$

This is the well known drift term in the Boltzmann transport theory, which in the present context describes the carrier acceleration within each miniband induced by the applied electric field $\mathbf{F}$.

The second term on the right-hand side of (10) cannot be treated exactly within our kinetic description. It is again the sum of two different contributions induced by carrier-phonon and carrier-light interactions, respectively:

$$\frac{d}{dt}f^{e/h}_{\mathbf{k}\nu}\Big|_{\mathbf{H}'} = \frac{d}{dt}f^{e/h}_{\mathbf{k}\nu}\Big|_{cp} + \frac{d}{dt}f^{e/h}_{\mathbf{k}\nu}\Big|_{cl}. \tag{12}$$

We will treat both terms within the standard semiclassical approximation and will not discuss the details of the derivation, which is similar to that contained in Ref. 23 for the case of a bulk semiconductor. Within such an approximation scheme a Markov limit is performed and therefore various memory effects are neglected. In particular energy-nonconserving transitions induced by a strong electric field,[25] i.e., intracollisional field effects, as well as time-energy uncertainty relation,[10,26] are not taken into account. However, the BO damping discussed in this paper is not particularly sensitive to such effects because they are of minor importance in determining the total carrier-phonon scattering rate.

The carrier-phonon contribution in (12) is given by the following rate equation:

$$\frac{d}{dt}f^{e/h}_{\mathbf{k}\nu}\Big|_{cp} = \sum_{\mathbf{k}'\nu'}\left[P^{e/h}_{\mathbf{k}\nu,\mathbf{k}'\nu'}f^{e/h}_{\mathbf{k}'\nu'} - P^{e/h}_{\mathbf{k}'\nu',\mathbf{k}\nu}f^{e/h}_{\mathbf{k}\nu}\right], \tag{13}$$

where $P^{e/h}_{\mathbf{k}\nu,\mathbf{k}'\nu'}$ is the carrier-phonon scattering rate for a transition from state $\mathbf{k}\nu$ to state $\mathbf{k}'\nu'$. It is easy to recognize the typical structure of the Boltzmann collision term, i.e., an in-scattering and an out-scattering contribution. Within our semiclassical approach, the explicit form of the above scattering rates is given by

$$P^{e/h}_{\mathbf{k}\nu,\mathbf{k}'\nu'} = \sum_{\pm}\frac{2\pi}{\hbar}\sum_{\mathbf{q}}|g^{e/h}_{\mathbf{k}'\nu',\mathbf{k}\nu;\pm\mathbf{q}}|^2\left(N_{\mathbf{q}}+\frac{1}{2}\mp\frac{1}{2}\right)$$
$$\times\left(1-f^{e/h}_{\mathbf{k}'\nu'}\right)\delta\left(\mathcal{E}^{e/h}_{\mathbf{k}'\nu'}-\mathcal{E}^{e/h}_{\mathbf{k}\nu}\pm\hbar\omega_{\mathbf{q}}\right), \tag{14}$$

where $N_{\mathbf{q}}$ is the phonon occupation number and the upper (lower) sign refers to phonon absorption (emission).

The typical structure of the above scattering rates results from Fermi's golden rule, i.e., they are proportional to the squared coupling matrix element g and they contain the Dirac δ function of energy conservation. The Pauli exclusion principle is reflected by the proportionality to the phase-space filling factor $1-f$ of the final state.

Finally, within our semiclassical approach the carrier-light contribution in (12) is described in terms of the electron-hole pair generation rate

$$\frac{d}{dt}f^{e/h}_{\mathbf{k}\nu}\Big|_{cl} = G^{e/h}_{\mathbf{k}\nu} = \sum_{\nu'}G^{e/h}_{\mathbf{k}\nu\nu'}, \tag{15}$$

where the summation runs over the optically coupled bands. For the case of Gaussian laser pulses, i.e., $E_0(t)=E_L e^{-(t/\tau_L)^2}$, the two-band generation rate has the following explicit form:

$$G^{e/h}_{\mathbf{k}\nu\nu'} = \frac{(2\pi)^{1/2}}{\hbar^2}|\mu_{\mathbf{k},\nu\nu'}E_L|^2\tau_L\exp\left[-2\left(\frac{t}{\tau_L}\right)^2\right]$$
$$\times\exp\left(-\frac{1}{2}(\tau_L\Delta\omega_{\mathbf{k},\nu\nu'})^2\right)(1-f^{e}_{\mathbf{k}\nu}-f^{h}_{\mathbf{k}\nu'}) \tag{16}$$

with $\hbar\Delta\omega_{\mathbf{k},\nu\nu'}=\mathcal{E}^{e}_{\mathbf{k}\nu}+\mathcal{E}^{h}_{-\mathbf{k}\nu'}-\hbar\omega_L$. Due to the Markov limit taken in the semiclassical approximation, the above generation rate (apart from the Pauli factor) is positive definite, i.e., there is no stimulated recombination as for the case of a fully coherent dynamics.[23,24] However, such a Markov limit still retains the time-energy uncertainty relation associated with the light-matter interaction.

By inserting the explicit form of the various contributions into (10), we can finally write down the set of coupled Boltzmann equations that govern the carrier dynamics in our semiconductor superlattice:

$$\frac{d}{dt}f^{e/h}_{\mathbf{k}\nu}+\frac{e^{e/h}\mathbf{F}}{\hbar}\cdot\nabla_{\mathbf{k}}f^{e/h}_{\mathbf{k}\nu}$$
$$= G^{e/h}_{\mathbf{k}\nu}+\sum_{\mathbf{k}'\nu'}\left[P^{e/h}_{\mathbf{k}\nu,\mathbf{k}'\nu'}f^{e/h}_{\mathbf{k}'\nu'}-P^{e/h}_{\mathbf{k}'\nu',\mathbf{k}\nu}f^{e/h}_{\mathbf{k}\nu}\right]. \tag{17}$$

In Sec. III, we will describe the Monte Carlo approach used to solve the above system of nonlinear equations. In our numerical analysis, we will determine the carrier wave functions and band structure of the superlattice within the following approximation scheme. The electronic states of the superlattice are computed within the effective-mass approximation from the familiar Kronig-Penney model, where the periodic potential is given as

an infinite sequence of identical quantum wells of width w separated by rectangular barriers of width b and height V_0, respectively (the superlattice period is $d = w + b$). Choosing the growth direction as the z axis of our coordinate system, we factorize the wave function as a product of a plane wave for the free particle motion in the x-y plane and a (super)lattice periodic, z-dependent function of Bloch type:

$$\Psi_{\mathbf{k}\nu}(\mathbf{r}) = \frac{1}{\sqrt{A}} e^{i\mathbf{k}_\perp \cdot \mathbf{r}_\perp} f_{k_z\nu}(z) \tag{18}$$

with

$$f_{k_z\nu}(z) = e^{ik_z z} u_{k_z\nu}(z) \ . \tag{19}$$

Here k_z varies in the superlattice Brillouin zone between $\pm\pi/d$. The properly normalized cell periodic Bloch factors $u_{\nu k_z}(z)$ are constructed by wave-function matching at the hetero-interfaces of the superlattice and by application of the appropriate periodic boundary conditions.[27] Neglecting nonparabolicity and nonsphericality of both conduction and valence bands, the corresponding energy dispersions of the superlattice minibands read

$$\mathcal{E}_{\mathbf{k}\nu} = \frac{\hbar^2 k_\perp^2}{2m^*} + \epsilon_{k_z\nu}, \tag{20}$$

where $\epsilon_{k_z\nu}$ is obtained by solving the following Kronig-Penney equation:

$$\cos k_z d = \cos \alpha w \cosh \beta b + \frac{(\gamma_B^2 - \gamma_W^2)}{2\gamma_B\gamma_W} \sin \alpha w \sinh \beta b, \tag{21}$$

with $\alpha = \sqrt{2m_W\epsilon/\hbar^2}$, $\beta = \sqrt{2m_B(V_0 - \epsilon)/\hbar^2}$, $\gamma_W = \alpha/m_W$, and $\gamma_B = \beta/m_B$. The effective mass m^* appearing in the in-plane part of the dispersion relation is a parameter that has to be related to the effective masses of the well and barrier materials m_W and m_B, respectively. As a result, our superlattice band structure is characterized by a cylindrical symmetry, i.e., it depends only on the parallel (k_z) and perpendicular ($k_\perp$) components of the three-dimensional wave vector $\mathbf{k}$.

Concluding this section, we will derive the explicit form of the carrier-phonon scattering rates (14) used in the Monte Carlo simulation. The functions $g^{e/h}$ introduced in (5) are defined as the matrix elements of the electrostatic phonon potential in the $\mathbf{k}\nu$ representation. The phonon system is described in terms of a single bulk LO-phonon mode and the matrix elements g are given by

$$g^{e/h}_{\mathbf{k}\nu,\mathbf{k}'\nu';\mathbf{q}} = \tilde{g}^{e/h}_{\mathbf{q}} \int d\mathbf{r} \Psi^{e/h*}_{\mathbf{k}'\nu'}(\mathbf{r}) e^{i\mathbf{q}\cdot\mathbf{r}} \Psi^{e/h}_{\mathbf{k}\nu}(\mathbf{r}) \ . \tag{22}$$

The coupling constants $\tilde{g}^{e/h}$ for the Fröhlich interaction with dispersionless bulk LO phonons of energy $\hbar\omega_0$ are identical for electrons and holes:

$$\tilde{g}_{\mathbf{q}} = g_0 \frac{1}{q} = \left[\frac{2\pi e^2 \hbar\omega_0}{V} \left(\frac{1}{\varepsilon_\infty} - \frac{1}{\varepsilon_s} \right) \right]^{1/2} \frac{1}{q} \ . \tag{23}$$

Here ε_∞ and ε_s denote the optical and the static dielectric constants of the effective medium and V is the normalization volume. We will consider only coupling to GaAs bulk phonons. This, of course, is a simplifying approximation that neglects any superlattice effect on the phonon dispersion, such as confinement of optical modes in the wells and in the barriers, and the presence of interface modes.[28] However, while these modifications have important consequences for phonon spectroscopies (such as Raman scattering), they are far less decisive for transport phenomena. Indeed, by now it is well known[28,29] that the total scattering rates are sufficiently well reproduced if the phonon spectrum is assumed to be bulklike.

The explicit evaluation of the Bloch matrix element in (22) yields first the conservation of the perpendicular momentum due to translational invariance: $\mathbf{k}_\perp - \mathbf{k}'_\perp = \pm\mathbf{q}_\perp$. Then, making use of the lattice periodicity of the Bloch functions $f_{k_z\nu}(z)$,[30] we may express the scattering rates (14) as a sum over reciprocal-lattice vectors $G = 2n\pi/d$ (with $n = 0, \pm1, \pm2, ...$):

$$P^{e/h}_{\mathbf{k}\nu,\mathbf{k}'\nu'} = \sum_{\pm} \frac{2\pi}{\hbar} g_0^2 \left(N_0 + \frac{1}{2} \mp \frac{1}{2} \right) \sum_G \frac{|\Phi^{\nu\nu'}_G(k_z, k'_z)|^2}{Q^2 + (\kappa + G)^2} \times \left(1 - f^{e/h}_{\mathbf{k}'\nu'} \right) \delta(\mathcal{E}_{\mathbf{k}\nu} - \mathcal{E}_{\mathbf{k}'\nu'} \pm \hbar\omega_0), \tag{24}$$

where we have introduced $\mathbf{Q} = \mathbf{k}_\perp - \mathbf{k}'_\perp$, $\kappa = k_z - k'_z$, and the Bloch integral

$$\Phi^{\nu\nu'}_G(k_z, k'_z) = \int_{\text{cell}} dz u_{k_z\nu}(z) u^*_{k'_z\nu'}(z) e^{iGz} \ .$$

Finally, the total scattering rates for intraminiband and interminiband processes are, as usual, obtained by summing the above transition probabilities over the final state wave vectors $\mathbf{k}'$:

$$\Gamma^{e/h}_{\nu\nu'}(\mathbf{k}) = \sum_{\mathbf{k}'} P^{e/h}_{\mathbf{k}\nu,\mathbf{k}'\nu'} \ . \tag{25}$$

III. MONTE CARLO PROCEDURE

In this section we will describe the Monte Carlo (MC) procedure used in our simulated experiments. As discussed in Sec. II, on a semiclassical level the carrier dynamics in our model of a semiconductor superlattice is described in terms of the coupled set of Boltzmann-like equations (17) for the various distribution functions $f^{e/h}_{\mathbf{k}\nu}$ in the different superlattice (SL) minibands:

$$\frac{d}{dt} f^{e/h}_{\mathbf{k}\nu} + \frac{e^{e/h}\mathbf{F}}{\hbar} \cdot \nabla_{\mathbf{k}} f^{e/h}_{\mathbf{k}\nu} = G^{e/h}_{\mathbf{k}\nu} + \frac{d}{dt} f^{e/h}_{\mathbf{k}\nu}\Big|_{cp} \tag{26}$$

(the last term is a shorthand notation for the carrier-phonon collision term).

Following the approach described in Ref. 31, we can introduce a coordinate transformation to a new set of variables, called "path variables":

$$\tilde{\mathbf{k}} = \mathbf{k} - \dot{\mathbf{k}}(t - t_0) \ , \tag{27}$$

with $\dot{\mathbf{k}} = \frac{e^{e/h}\mathbf{F}}{\hbar}$, and a corresponding transformed distribution function $\tilde{f}$ defined by

$$\tilde{f}^{e/h}_{\tilde{\mathbf{k}}\nu} = f^{e/h}_{\mathbf{k}\nu} \ . \tag{28}$$

This transformation eliminates the drift term on the left-hand side of Eq. (26):

$$\frac{d}{dt}\tilde{f}^{e/h}_{\tilde{\mathbf{k}}\nu} = \tilde{G}^{e/h}_{\tilde{\mathbf{k}}\nu} + \frac{d}{dt}\tilde{f}^{e/h}_{\tilde{\mathbf{k}}\nu}\Big|_{cp} \ , \tag{29}$$

where $\tilde{G}$ denotes the transformed generation rate. The acceleration induced by the applied electric field, previously described by the drift term, is now implicitly contained in $\tilde{\mathbf{k}}$, i.e., $\tilde{\mathbf{k}}$ is a function of time [see Eq. (27)]. In the absence of carrier photogeneration and carrier-phonon scattering, the transformed distribution function $\tilde{f}$ is constant in time and therefore from Eq. (28) we obtain

$$f^{e/h}_{\mathbf{k}\nu}(t) = f^{e/h}_{\mathbf{k}-\dot{\mathbf{k}}(t-t_0),\nu}(t_0) \ . \tag{30}$$

This is known as the "acceleration theorem."

Within our approach, the system of nonlinear equations (29) is solved in terms of a direct MC simulation of the carrier dynamics in this transformed $\tilde{\mathbf{k}}$ space. Following the spirit of the number representation introduced in Ref. 23 for a bulk system, we use a suitable $\mathbf{k}$-space discretization. In particular, due to the symmetry of our system, we define a cylindrical (two-dimensional) grid and for each cell of the grid we introduce an integer number $n^{e/h}_{i\nu}$, which denotes the number of carriers in the ith cell and miniband ν. As for the bulk case, this representation provides a direct way of treating both the carrier photogeneration and the carrier-phonon scattering.

Due to the dependence of the scattering rates on the distribution functions, the set of kinetic equations (29) is nonlinear and therefore we are forced to perform a time step solution. In particular, we employ a fixed time step Δt over which our kinetic equations are locally linear and decoupled.

As discussed before, in Eq. (29) the effect of the external field is implicitly contained in the time dependence of $\tilde{\mathbf{k}}$. This is easily included in our MC simulation by considering our grid not in $\mathbf{k}$ but in $\tilde{\mathbf{k}}$ space, i.e., by introducing a time-dependent grid that drifts according to (27). Therefore, at each time step, the original distribution function f appears to drift due to a constant shift of the grid. During the time step, the carrier photogeneration and carrier-phonon terms in Eq. (29) are evaluated by means of a traditional MC simulation: given the carrier distribution at the beginning of the time step in terms of the occupation numbers $n^{e/h}_{i\nu}$, we generate for each particle a random sequence of free flights and scattering events[13] according to the various scattering rates in Eqs. (25) and (24).

Since the effect of the external field has been already taken into account by shifting the grid in $\mathbf{k}$ space, there is no additional acceleration by the external field during the free flight. Therefore, the scattering rates are constant in time and there is no need for any self-scattering technique.

Our MC procedure can then be summarized as follows. The total simulation time is divided into a sequence of time steps. For each of them (i) We create the new electron-hole pairs over the grid in $\mathbf{k}$ space according to the generation rate in Eq. (15); (ii) we generate a random sequence of free flights and scattering events for each carrier in the various minibands, the result being a random walk both over $\mathbf{k}$ and over the different minibands, and (iii) the grid in $\mathbf{k}$ space is shifted according to the applied electric field at the end of the time step and the distribution function is updated on the new grid.

IV. NUMERICAL RESULTS

In this section we present the results of our Monte Carlo simulations. We start with a discussion of the band structure and the intraminiband and interminiband scattering rates for LO-phonon emission of a particular $GaAs/Al_xGa_{1-x}As$ superlattice. All our simulations were performed assuming a lattice temperature of 10 K and low carrier densities. At this low temperature the rates for the LO-phonon absorption are very small. We study the relaxation of energetically high excited electrons due to LO-phonon scattering. We then investigate the influence of an applied electric field on the electronic distribution function. Assuming carrier excitation at the band edge, the electric field leads to BO's performed by the electrons. Since the width of the lower electronic miniband of the considered structure is smaller than the LO-phonon energy, the BO's are not damped by this scattering mechanism. Therefore the charge current will show periodic oscillations in time, which give rise to an emitted radiation.

In the next step we then present results on the combined effect of an electric field and LO-phonon scattering, assuming carrier excitation high in the band. The amplitude of the BO decreases in time due to intraminiband and interminiband LO-phonon scattering. In Sec. IV E we consider a superlattice model where the miniband width of the lower electronic band is larger than the LO-phonon energy. We discuss the intraminiband scattering rates and show that, in agreement with the experimental observation, the BO's in this structure are intrinsically damped due to LO-phonon emission.[15]

A. Band structure and scattering rates

For our analysis of relaxation and field-induced phenomena, we assume the following structural parameters: a $GaAs/Al_{0.3}Ga_{0.7}As$ superlattice, with 95-Å-well and 15-Å-barrier widths. The confinement potential for the electrons (holes) is 250 meV (123 meV). The effective mass for electrons in the well (barrier) material is $0.067m_0$ ($0.092m_0$). The corresponding value for the heavy hole is $0.38m_0$ ($0.41m_0$). In the perpendicular direction we have chosen the effective mass $0.070m_0$ ($0.38m_0$) for the electrons (holes). The light holes have been neglected for simplicity.

Figure 1 shows the band structure in the growth direction of the first two (a) electron and (b) heavy-hole minibands, which have been calculated within the Kronig-Penney model. The miniband widths are 21 and 75 meV for the electrons, and 2 and 7 meV for the holes. The width of the lower electronic miniband in this structure is therefore smaller than the LO-phonon energy of 36.4 meV. Consequently, LO-phonon emission is suppressed for states in this miniband, provided the kinetic energy of the perpendicular motion $E_\perp$ is small.

In Fig. 2(a) the carrier scattering rate is plotted as a function of the miniband energy E_z for different values of $E_\perp$. For $E_\perp = 0$ the rate vanishes within the entire miniband. For $E_\perp = 25$ meV the LO-phonon emission process can take place only for E_z larger than approximately 11 meV. However, the emission process is possible for all E_z if $E_\perp$ exceeds the LO-phonon energy. The corresponding rate for $E_\perp = 50$ meV has a maximum value of about 5.5 ps^{-1} at $E_z \approx 8$ meV. This maximum corresponds to transitions to the states at the upper edge of the miniband with $E_\perp = 0$ and reflects the superlattice density of states.

The scattering rates for the higher electronic miniband are shown in Fig. 2(b) for $E_\perp = 0$. Since the width of this miniband is larger than the LO-phonon energy, the intraminiband scattering rate shows the expected threshold behavior as a function of E_z. The interminiband scattering [see Fig. 2(b) dashed line], is different from zero over the entire energy range. On average, this rate is about a factor of 3 smaller than the rate for intraminiband transitions since the wave functions in adjacent minibands have different symmetry and the resulting overlap is small.

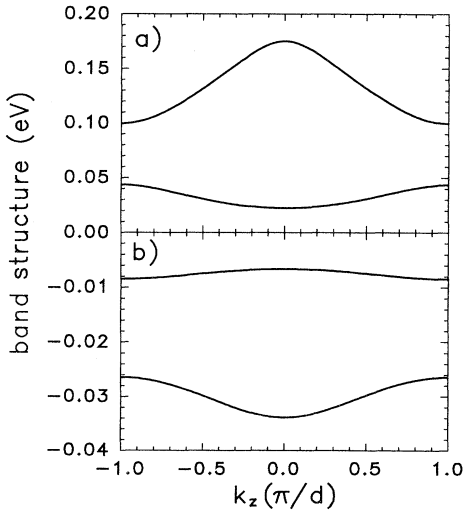

FIG. 1. (a) Energy dispersion of the two lowest electronic minibands of the first structure, a $GaAs/Al_{0.3}Ga_{0.7}As$ superlattice, with a 95-Å-well and a 15-Å-barrier width. k_z is the wave-vector component in the growth direction. (b) Energy dispersion of the first two hole minibands of the same structure. The zero of the energy scale corresponds to the bottom of the well potential.

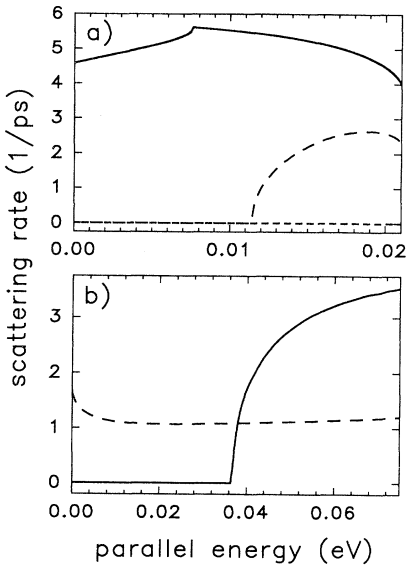

FIG. 2. (a) Intraminiband-scattering rate within the lower electronic miniband, as a function of the parallel energy E_z for different values of the transverse energy: $E_\perp = 0$ (short dashed), $E_\perp = 25$ meV (long dashed); $E_p = 50$ meV (solid). (b) Intraminiband scattering rate within the higher electronic miniband for $E_\perp = 0$, as a function of the parallel energy (solid), and interminiband scattering rate from higher to lower band for $E_\perp = 0$ (dashed).

B. Relaxation regime

Let us now turn to the relaxation of photoexcited carriers due to LO-phonon scattering. Here and in the following a laser pulse width of $\tau_L = 100$ fs has been assumed. The laser pulse is centered at $t = 0$ and creates electrons with an excess energy of about 150 meV with respect to the bottom of the well. Such a pulse creates a superposition of electrons in both minibands [see Fig. 1(a)]. The time evolution of the carrier distribution as a function of the total energy is plotted in Fig. 3. At $t = 0$ the distribution function consists of the dominant generation peak and a small contribution, which is located energetically one LO phonon below the initial peak. For times longer than 200 fs we recognize the well known phonon replicas whose amplitudes change in time due to relaxation processes. Finally, after about 2 ps almost all carriers have relaxed in energy as far as they can. An interesting feature in Fig. 3 is that starting from $t = 600$ fs, when the third phonon replica around 0.04 meV is the largest peak, the first replica slightly above 0.11 meV is stronger than the second one. This is explained by the fact that the energetic position of the first phonon replica is within the higher miniband. Since the interminiband scattering rates are smaller than the intraminiband rates, the strength of the first replica at higher times reflects the population of the higher miniband.

The carrier densities for the different minibands are shown in Fig. 4(a) as a function of time. After the end of the laser pulse, the total density is constant, about 1.2×10^{14} cm^{-3}. At $t = 0$ the carrier density in the

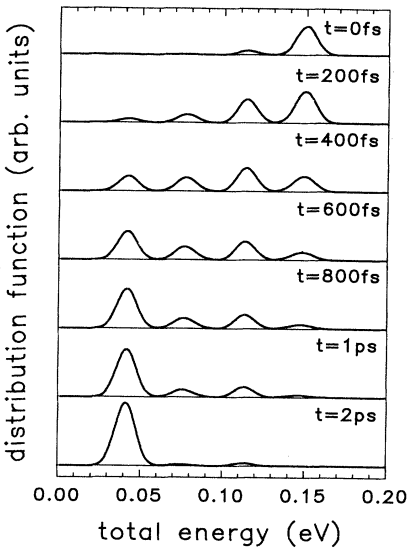

FIG. 3. Electron distribution in the first superlattice structure as a function of the total energy at different times (t=0,0.2,0.4,0.6,0.8,1.0,2.0 ps). Energies are referred to the bottom of the well. The laser pulse (pulse width $\tau_L = 100$ fs) initially creates electrons around 150 meV.

higher miniband is about half of that excited in the lower one. Due to interminiband scattering, the density in the higher miniband later decreases in time and, correspondingly, the density in the lower miniband increases.

In Fig. 4(b) the mean kinetic energies of the electrons in the two minibands are plotted as function of time. The kinetic energy relaxes from its initial value in about 1 ps to an almost constant value, which is smaller than the LO-phonon energy.

C. Transport regime (BO)

For the studies in this section we now include an electric field, applied parallel to the growth direction, and study its influence on the dynamics of the distribution function. For this simulated experiment, the central energy of the laser pulse is assumed to be located 8 meV below the band gap energy. Figure 5 shows the time evolution of the carrier distribution for an electric field of 5 kV/cm as a function of k_z, i.e., averaged over $k_\perp$. At the beginning of the laser pulse the carriers are generated around $k_z = 0$, where the transitions are close to resonance with the laser excitation. According to the acceleration induced by the field, the electrons are then shifted in k space. When the carriers reach the border of the first Brillouin zone they are Bragg reflected. After 800 fs, which is close to the BO time $T_B = h/eFd = 750$ fs, the carriers have completed a little more than one oscillation in k space (see Fig. 5). Since the electrons have been excited at the bottom of the miniband and the miniband width is smaller than the LO-phonon energy, no LO-phonon emission is possible in this case. Consequently, the electrons perform BO's without losing the synchronicity of their motion by scattering. This is shown in Fig. 6, where we have plotted the mean kinetic energy [Fig. 6(a)], the current [Fig. 6(b)], which is given by $j_\nu^e(t) = \frac{e}{\hbar}\int \frac{\partial \epsilon_{k_z\nu}}{\partial k_z} f^e_{\mathbf{k}\nu} d\mathbf{k}$, and its derivative with respect to time, which is proportional to the emitted electric far field, i.e., the terahertz signal [Fig. 6(c)].[18] All

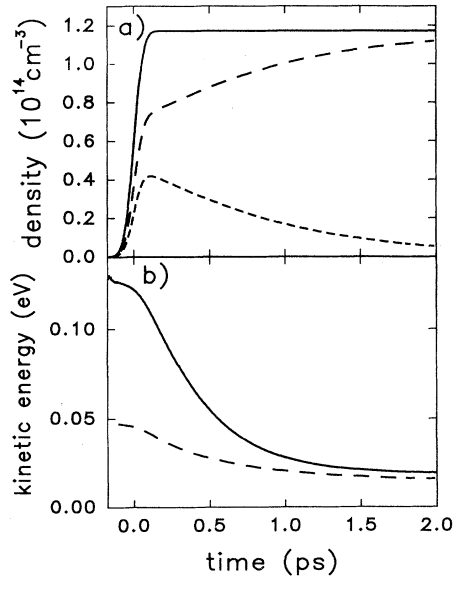

FIG. 4. (a) Density in the two electronic minibands as a function of time: higher miniband (short dashed), lower miniband (long dashed), and sum of both (solid). (b) Average kinetic energies in the different minibands as a function of time: higher miniband (long dashed) and lower miniband (solid).

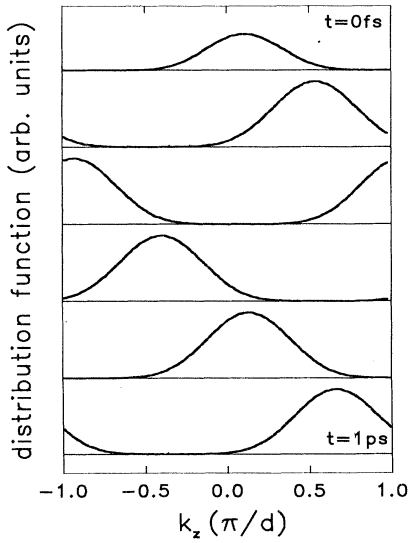

FIG. 5. Electron distribution in the first superlattice structure as a function of k_z at different times (t=0,0.2,0.4,0.6,0.8,1.0 ps), under an applied electric field of 5 kV/cm. The laser pulse (pulse width $\tau_L = 100$ fs) is centered 8 meV below the band gap.

these quantities show oscillations with the BO periodicity. As expected, the amplitude of the oscillations of the kinetic energy [Fig. 6(a)] is somewhat smaller than the miniband width. Since no scattering is present the oscillations of the current [Fig. 6(b)] are symmetric around zero, i.e., the average current vanishes. The oscillations of the terahertz signal are not symmetric with respect to positive and negative values. This is explained by the fact that the band structure in the growth direction has different curvatures at the upper and lower miniband edges. When electrons are excited in the vicinity of the lower band edge, the shape of one temporal oscillation of the terahertz signal is approximately proportional to the second derivative of the dispersion.

D. Combined influence of relaxation and transport

In this section we study the combined influence of the relaxation and the electric field on the dynamics of the carrier distribution function. The electrons are again assumed to be excited with an excess energy of about 150 meV. The time evolution of the distribution function is shown in Fig. 7. At $t = 0$, which corresponds to the center of the laser pulse, the distribution function shows a peak energetically located at the excitation energy and a small structure about one LO-phonon energy below. For times between 200 fs and 1 ps the electrons relax

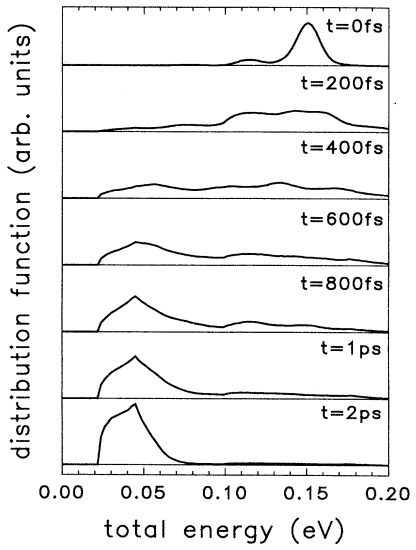

FIG. 7. Electron distribution in the first superlattice structure as a function of the total energy at different times (t=0,0.2,0.4,0.6,0.8,1.0,2.0 ps). Energies are referred to the bottom of the well. The laser pulse (pulse width $\tau_L = 100$ fs) initially creates electrons around 150 meV. The intensity of the applied electric field is 5 kV/cm.

in energy due to phonon emission. Due to the action of the electric field, the LO-phonon replica is strongly broadened and almost invisible in Fig. 7. After 2 ps the carriers have relaxed in energy as much as possible under the given circumstances. Due to the influence of the electric field, the distribution is much broader as compared to Fig. 3. Some of the carriers were able to relax to states that are lower in energy than in the case without field.

Figure 8(a) shows the time dependence of the averaged kinetic energies in the two minibands. While the kinetic energy of the carriers in the lower miniband decreases monotonously in time, the kinetic energy for the higher miniband exhibits the typical time periodicity induced by BO's. Since the width of the higher miniband is larger than both the LO-phonon energy and the width of the lower miniband, the electrons can gain more energy due to the field-induced acceleration and lose it again by LO-phonon emission. For the conditions chosen in our simulations the BO time and the average LO-phonon scattering time are comparable. This explains the high average kinetic energy of the electrons in the higher miniband after the oscillations have been damped. In Fig. 8(b) the corresponding charge currents of the two minibands are shown. The current of the higher miniband oscillates with the BO time of about 750 fs. The scattering leads to a strong damping of these oscillations. The current of the lower miniband shows only weak oscillations, which are phase shifted by approximately π with respect to the oscillations in the higher miniband. The exact value of this phase shift is determined by the strength of the scattering and the value of the electric field. Since the scattering is active, we have a positive average current.

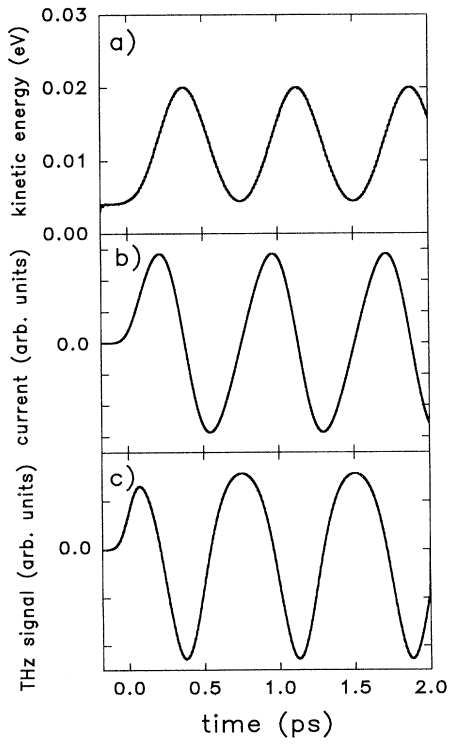

FIG. 6. (a) Average kinetic energy, (b) current, and (c) terahertz signal corresponding to the lower electronic miniband as a function of time. The laser pulse (pulse width $\tau_L = 100$ fs) is centered 8 meV below the band gap. The intensity of the applied electric field is 5 kV/cm.

The corresponding terahertz signals are shown in Fig. 8(c). For the higher miniband the signal shows strongly damped BO's, while for the lower miniband the signal is only very weakly modulated.

E. Damping of BO

Finally, we present calculations assuming a slightly different superlattice structure with composition identical to the previous one, but different structural parameters: wells and barriers have an equal width of 30 Å. The effective masses in the perpendicular direction have been chosen to be $0.077m_0$ ($0.39m_0$) for the electrons (holes). Since the period of this superlattice is much smaller than that of the former one the minibands are more dispersive. We obtain a bandwidth of about 62 meV for the first electron and 5 meV for the first hole miniband, respectively. Thus the width of the electronic miniband is larger than the LO-phonon energy and intraminiband phonon scattering can take place in this structure even for $E_\perp = 0$. The calculated scattering rates for LO-phonon emission within the electronic miniband are shown in Fig. 9. As expected, we find for $E_\perp = 0$ a sharp threshold at $E_z = \hbar\omega_0$. Therefore, as a consequence of the phonon scattering BO's in this structure will be damped for any excitation condition. The threshold for $E_\perp = 25$ meV is reduced again to about 11 meV and the rates are somewhat larger compared to the case of $E_\perp = 0$. For $E_\perp = 50$ meV there is no threshold at all and the scattering rates are further increased.

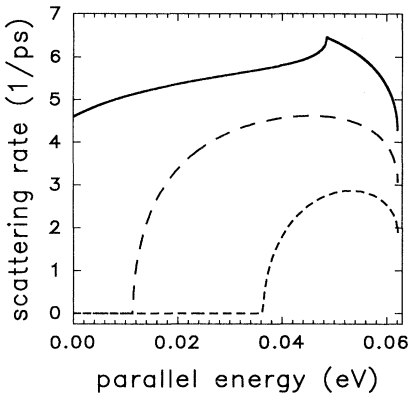

FIG. 9. Intraminiband scattering rate within the electronic miniband as function of the parallel energy E_z for different values of the transverse energy, for a $GaAs/Al_{0.3}Ga_{0.7}As$ superlattice, with a 30-Å-well and a 30-Å-barrier width: $E_\perp = 0$ (short dashed), $E_\perp = 25$ meV (long dashed), and $E_\perp = 50$ meV (solid).

Figure 10 displays the temporal evolution of the electron distribution as a function of k_z. The central laser frequency was assumed to be tuned to 8 meV below the band gap and the electric field was chosen to be 9.2 kV/cm, which gives again a BO period of 750 fs. As in Fig. 5, the distribution is generated around $k_z = 0$ at the beginning of the laser pulse and subsequently shifted in k space by the electric field. For $t = 400$ fs the shape of the distribution is strongly distorted by LO-phonon emission, which now can take place since the carriers have gained

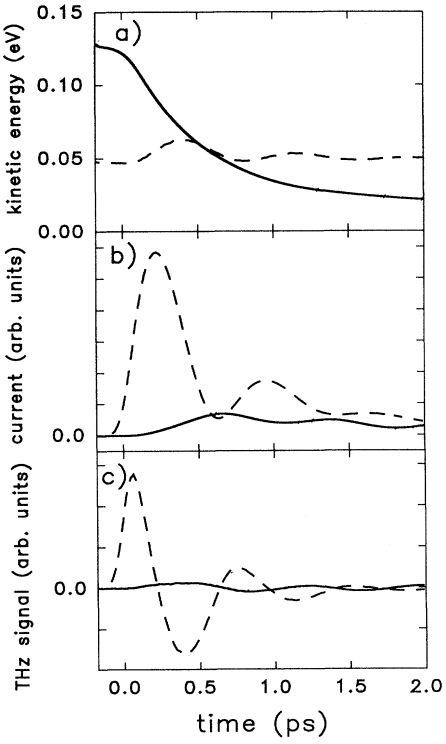

FIG. 8. (a) Average kinetic energy, (b) current, and (c) terahertz signal corresponding to the lower (solid line) and the higher (dashed line) electronic minibands as a function of time. The intensity of the applied electric field is 5 kV/cm.

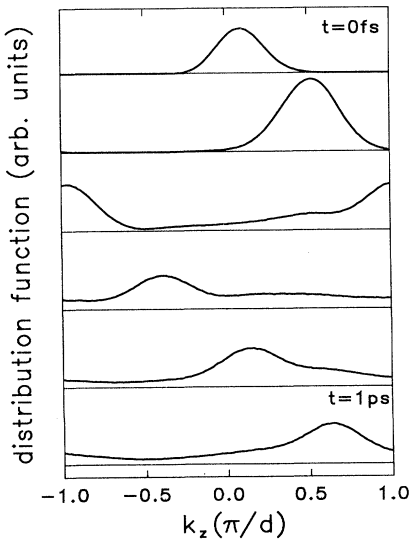

FIG. 10. Electron distribution in the second superlattice structure as a function of k_z at different times (t=0,0.2,0.4,0.6,0.8,1.0 ps), under an applied electric field of 9.2 kV/cm. The laser pulse (pulse width $\tau_L = 100$ fs) is centered 8 meV below the band gap.

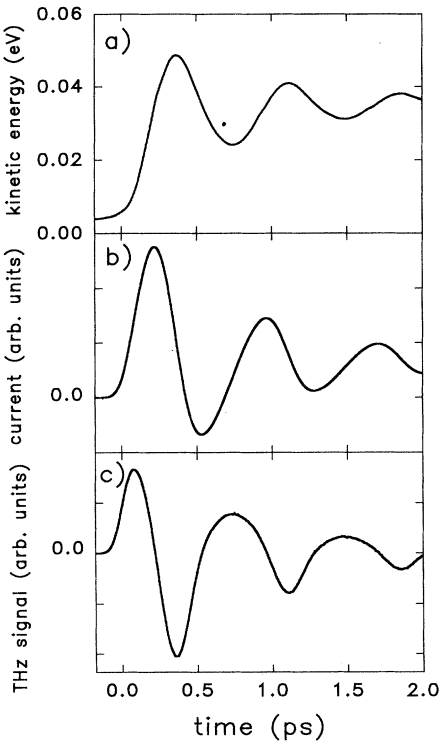

FIG. 11. (a) Average kinetic energy, (b) current, and (c) terahertz signal from the electrons in the second superlattice structure as a function of time. The intensity of the applied electric field is 9.2 kV/cm.

enough kinetic energy from the applied field. Therefore the carriers are scattered from high energies, i.e., large k_z values, to the bottom of the miniband, i.e., $k_z \approx 0$. For longer times only that fraction of carriers that has not been scattered gives rise to BO. This damping of the BO due to the LO-phonon emission is also visible in the plots of the kinetic energy, the current, and the terahertz signal [Figs. 11(a)–11(c)]. The kinetic energy initially increases and then oscillates with the BO period and a decreasing amplitude around an average value of about 35 meV. The current and the terahertz signal [Figs. 11(b) and 11(c)] also show damped oscillations in time. Again, the terahertz signal is found to be asymmetric with respect to its positive and negative parts due to the different curvatures at the upper and the lower miniband edges.

Comparing the BO features of the distribution function for the two SL's, the following summary can be drawn. In the first superlattice structure the width of the lower electronic miniband is smaller than the LO-phonon energy. For optical excitations at the lower band edge the BO's are not damped by LO-phonon emission, which cannot occur as a consequence of energy conservation. The second superlattice structure has a miniband width that is larger than $\hbar\omega_0$: the BO's are strongly damped by scattering. These results agree qualitatively with experiments on BO's in superlattice samples with the same structural parameters we have chosen here[5,15] and substantiate our previous qualitative arguments.[15]

V. CONCLUSIONS

In summary, we have presented a detailed investigation of the ultrafast dynamics of photoexcited carriers in semiconductor superlattices. Our theoretical analysis is based on a direct simulation of the carrier dynamics corresponding to a Monte Carlo solution of a coupled set of Boltzmann-like equations for the carrier distributions in the various electron and hole minibands.

We have focused our attention on the low-temperature and low-density regime where the most relevant scattering mechanism is LO-phonon emission. The threshold nature of this scattering mechanism was found to play a decisive role for the relaxation and transport properties of the superlattices. In particular, the damping of Bloch oscillations is directly related to the width of the superlattice miniband compared to the LO-phonon energy. For laser excitations close to the bottom of a miniband with a width smaller than the LO-phonon energy, we obtain basically undamped Bloch oscillation behavior. Conversely, for laser excitation far from the band gap and/or miniband widths larger than the LO-phonon energy, these oscillations are strongly damped. The resulting average current is different from zero and dissipation takes place.

The kinetic treatment, typical for any Monte Carlo simulation, allowed us to study the role of the different intraminiband and interminiband LO-phonon scattering processes. As expected, interminiband scattering is slower than scattering within the minibands and thus of minor importance for Bloch oscillations.

Finally, the number representation used in the Monte Carlo simulation allows us in principle to treat also coherent phenomena as well as carrier-carrier Coulomb scattering. Therefore, the described simulation method can be regarded as the starting point for a generalized Monte Carlo simulation of both coherent and incoherent phenomena in semiconductor superlattices.

ACKNOWLEDGMENTS

We are grateful to S.M. Goodnick, M. Gulia, and G. von Plessen for stimulating and useful discussions. This work was supported in part by the EC Commission through the Network "ULTRAFAST" and by the Deutsche Forschungsgemeinschaft through the Sonderforschungsbereich 383.

[1] J. Shah, Solid State Electron. **32**, 1051 (1989).
[2] T. Elsaesser, J. Shah, L. Rota, and P. Lugli, Phys. Rev. Lett. **66**, 1757 (1991).
[3] J.A. Kash, in *The Physics of Semiconductors*, edited by E. M. Anastassakis and J.D. Joannopoulos (World Scientific, Singapore, 1990), p. 2459.
[4] C.W.W. Bradley, R.A. Taylor, and J.F. Ryan, Solid State Electron. **32**, 1173 (1989).

[5] J. Feldmann *et al.*, Phys. Rev. B **46**, 7252 (1992).
[6] C. Waschke *et al.*, Phys. Rev. Lett. **70**, 3319 (1993).
[7] D.C. Scott, R. Binder, and S.W. Koch, Phys. Rev. Lett. **69**, 347 (1992).
[8] R. Binder *et al.*, Phys. Rev. B **45**, 1107 (1992).
[9] M. Hartmann and W. Schäfer, Phys. Status Solidi B **173**, 165 (1992).
[10] D.B. Tran Thoai and H. Haug, Phys. Rev. B **47**, 3574 (1993).
[11] S.M. Goodnick and P. Lugli, in *Hot Carriers in Semiconductor Nanostructures: Physics and Applications*, edited by J. Shah (Academic, New York, 1992), pp. 191–234.
[12] M.H. Kalos and P.A. Whitlock, *Monte Carlo Method Vol. 1: Basics* (Wiley, New York, 1986).
[13] C. Jacoboni and P. Lugli, *The Monte Carlo Method for Semiconductor Device Simulation* (Springer, Wien, 1989).
[14] J. Lary and S.M. Goodnick, SPIE **1675**, 22 (1992).
[15] G. von Plessen *et al.*, Phys. Rev. B **49**, 14 058 (1994).
[16] W. Quade, E. Schöll, F. Rossi, and C. Jacoboni, Phys. Rev. B **50**, 7398 (1994).
[17] F.M. Bufler and J. Schlösser, J. Phys. Condens. Matter **6**, 7445 (1994); Phys. Rev. B **51**, xxx (1995).
[18] T. Meier, G. von Plessen, P. Thomas, and S.W. Koch, Phys. Rev. Lett. **73**, 902 (1994); Phys. Rev. B **51**, 14 490 (1995).
[19] S. Schmitt-Rink, D.S. Chemla, and H. Haug, Phys. Rev. B **37**, 941 (1988).
[20] M. Lindberg and S.W. Koch, Phys. Rev. B **38**, 3342 (1988).
[21] H. Haug and S.W. Koch, *Quantum Theory of the Optical and Electronic Properties of Semiconductors*, 3rd ed. (World Scientific, Singapore, 1994).
[22] Y.Z. Hu, R. Binder, and S.W. Koch, Phys. Rev. B **47**, 15 679 (1993).
[23] T. Kuhn and F. Rossi, Phys. Rev. Lett. **69**, 977 (1992); Phys. Rev. B **46**, 7496 (1992).
[24] F. Rossi, S. Haas, and T. Kuhn, Phys. Rev. Lett. **72**, 152 (1994).
[25] R. Brunetti, C. Jacoboni, and F. Rossi, Phys. Rev. B **39**, 10 781 (1989).
[26] J. Schilp, T. Kuhn, and G. Mahler, Phys. Rev. B **50**, 5435 (1994).
[27] G. Bastard, *Wave Mechanics Applied to Semiconductor Heterostructures* (Les Editions de Physique, Paris, 1988).
[28] E. Molinari, in *Confined Electrons and Photons: New Physics and Applications*, edited by E. Burstein and C. Weisbuch (Plenum, New York, 1994).
[29] H. Rücker, E. Molinari, and P. Lugli, Phys. Rev. B **45**, 6747 (1992).
[30] P.J. Price, Ann. Phys. (N.Y.) **133**, 217 (1981).
[31] F. Rossi, P. Poli, and C. Jacoboni, Semicond. Sci. Technol. **7**, 1017 (1992).